Unravelling Middle to Late Jurassic palaeoceanographic and palaeoclimatic signals in the Hebrides Basin using belemnite clumped isotope thermometry

Madeleine L. Vickers[1*], Alvaro Fernandez[2], Stephen P. Hesselbo[3], Gregory D. Price[4], Stefano M. Bernasconi[5], Stefanie Lode[6], Clemens V. Ullmann[3], Nicolas Thibault[1], Iben Winther Hougaard[1]; Christoph Korte[1]

[1]University of Copenhagen, Faculty of Science, Geology Section, Øster Voldgade 10, DK-1350 Copenhagen K, Denmark

[2]Bjerknes Centre for Climate Research and Department of Earth Science, University of Bergen, Allégaten 41, N-5007 Bergen, Norway

[3]Camborne School of Mines, University of Exeter, Penryn Campus, Penryn, Cornwall TR10 9FE, U.K.

[4]School of Geography, Earth and Environmental Sciences, Plymouth University, Drake Circus, Plymouth, PL4 8AA, U.K.

[5]ETH Zürich, Geologisches Institut, Sonneggstrasse 5, 8092 Zürich, Switzerland

[6]Geological Survey of Denmark and Greenland, Department of Petrology and Economic Geology, Øster Voldgade 10, DK-1350 Copenhagen K, Denmark

*corresponding author: mlv@ign.ku.dk

Keywords: Jurassic palaeoclimate; belemnites; palaeoceanography; clumped isotopes

Abstract

Clumped isotope based temperature estimates from exceptionally well-preserved belemnites from Staffin Bay (Isle of Skye, Scotland) reveal that seawater temperatures throughout the Middle-Late Jurassic were significantly warmer than previously reconstructed by conventional oxygen isotope thermometry. We demonstrate here that this underestimation by oxygen isotope thermometry was likely due to a) using the incorrect calcite thermometry equation for belemnite temperature reconstructions and b) by incorrectly estimating the seawater $\delta^{18}O$ ($\delta^{18}O_{sw}$) for the Hebrides basin.

Our data suggests that the fractionation factor for oxygen isotopes in belemnites from seawater was closer to that of slow-growing abiogenic calcites than that of other marine calcifying organisms. Our clumped isotope temperatures are used to reconstruct $\delta^{18}O_{sw}$ trends across the Callovian–Kimmeridgian in the Hebrides Basin. The $\delta^{18}O_{sw}$ varied significantly in the Hebrides Basin throughout this interval, possibly as a result of changing currents through the Laurasian seaway. Trends in temperature and $\delta^{18}O_{sw}$ are compared to published palaeoceanographic studies to shed light on changing palaeoceanography in the Tethyan and Boreal realms throughout the Middle–Late Jurassic.

Keywords: Jurassic palaeoclimate; belemnites; palaeoceanography; clumped isotopes

1. Introduction

Understanding global and local climate during the Jurassic greenhouse (201.3-145.0 Ma) is of great interest and importance, as this period, during which carbon dioxide levels are thought to have been more than five times higher than pre-industrial levels (Berner and Kothavala, 2001), may represent an alternative stable state of Earth's climate at conditions similar to projected future atmospheric CO_2 levels. In order to predict future global and local climatic regimes under such high atmospheric CO_2 levels, it is necessary to understand how the Earth has responded previously to such conditions. Difficulties arise in reconstructing Jurassic climate and carbon cycle changes, as many conventional climate proxies (e.g. biomarker-based temperature reconstructions) do not extend back so deep in time (e.g. Brassel, 1986; deBar et al., 2019). Oxygen isotope thermometry of biogenic calcite is one of the commonly used proxies for examining such deep time palaeoclimate, although there are a number of limitations and caveats to this method. It is important that the calcite chosen for the study is (1) well preserved, (2) secreted in equilibrium with the surrounding seawater. Belemnite rostra (the calcitic hardpart of this extinct cephalopod group) have been commonly used in numerous

Jurassic and Cretaceous climate studies to reconstruct marine temperatures via oxygen isotope thermometry ($\delta^{18}O_{belemnite}$, e.g. Podlaha et al., 1998; Wierzbowski, 2004; Bailey et al., 2003; Nunn et al., 2009; Korte et al., 2015; Price et al., 2015), as they are abundant throughout this period, and widespread over a broad range of latitudes. However, there are several confounding factors that can lead to difficulty in interpreting trends in the Jurassic belemnite record. Firstly, belemnites may exhibit a fractionation different to that of the (most commonly used) oxygen isotope temperature equations which were empirically derived for modern biotic (e.g. Epstein et al., 1953; Shackleton, 1974; Killingley and Newman, 1982; Brand et al., 2013) or abiotic (e.g. Kim and O'Neil, 1997; Coplen, 2007; Kele et al., 2015; Daëron et al., 2019) calcite. As belemnites are extinct, it is not possible to measure their specific fractionation factor, and there is debate as to whether belemnite calcite was grown in equilibrium with seawater (e.g., Voigt et al., 2003; Price et al., 2015; Stevens et al., 2017). Secondly, oxygen isotope temperature reconstructions require knowledge of the $\delta^{18}O$ value of the seawater from which the calcite precipitated ($\delta^{18}O_{sw}$). Mesozoic temperature studies commonly assume a $\delta^{18}O_{sw}$ = -1 ‰, the global average for an ice-free world (Shackleton and Kennett, 1975). However, this assumption is a gross estimate that bears large uncertainties since the $\delta^{18}O_{sw}$ of the modern oceans is measurably variable by up to 10 ‰, depending on depth, and local evaporation and runoff balances (e.g. LeGrande and Schmidt, 2006), and ancient oceans are likely to have exhibited the same heterogeneity (e.g. Zhou et al., 2008). Moreover, there is limited knowledge of belemnite life habits, i.e. what depth they inhabited, and whether or not they were migratory. Much of what is thought to be known about belemnite habitat depth and migration patterns comes from studying the sedimentological evidence (i.e. which facies associations they are found in), examination of their nearest living relatives, and belemnite rostrum morphology and geochemistry, but this evidence has led to contradictory conclusions, and may reflect differences between belemnite species or genera. In general, it is now considered that belemnites inhabited the well-oxygenated, top 200 m of the water column, in shallow marine, hemipelagic shelf environments, in order to support their active swimming, predatory lifestyle (Hoffmann and Stevens, 2019 and references therein). Within these limits, different belemnite genera are thought to have inhabited different niches, i.e. different water temperatures and depths (Hoffmann and Stevens, 2019).

Clumped isotope thermometry offers a solution to the problem of reconstructing marine temperatures from belemnites by reconstructing calcite precipitation temperatures independently of the $\delta^{18}O_{sw}$. This proxy measures the temperature-dependent enrichment of ^{18}O-^{13}C bonds over a stochastic distribution in the carbonate molecule. At thermodynamic equilibrium, the clumped isotope composition (Δ_{47}) of the measured carbonate should be solely a function of the carbonate precipitation temperature (e.g., Eiler, 2007). Temperatures derived from this method can then be used in combination with conventional oxygen isotope measurements to reconstruct the $\delta^{18}O_{sw}$ from which the calcite precipitated (e.g., Came et al., 2007; Price and Passey, 2013; Wierzbowski et al., 2018; Vickers et al., 2019).

In this study, we apply clumped isotope thermometry to exceptionally well-preserved belemnite rostra from the Middle- to Late Jurassic succession of Staffin Bay, Trotternish Peninsula, Isle of Skye, Scotland in order to improve understanding of belemnite life habits and reconstruct changes in temperatures and $\delta^{18}O_{sw}$ throughout this interval. We analyse two belemnite genera, *Pachyteuthis* and *Cylindroteuthis*, to see if there are any significant difference between them arising from different general life habits or vital effects. It has been suggested that *Pachyteuthis*, with its short, thick rostum, may represent a more nektobenthic lifestyle (Mutterlose et al., 2010). *Cylindroteuthis* may have lived in an offshore habitat, possibly living in deeper hemipelagic environments (95 – 189 m; Matrill et al., 1994; Hewitt, 2000).

1.1 Geological Setting

During the Jurassic, the Isle of Skye was part of the Hebrides Basin (palaeolatitude *c.* 40 °N, Fig. 1), a half-graben that formed, along with a number of basins on the Atlantic margin, during the early extensional phases of the evolution of the Central and North Atlantic Oceans (Morton and Hudson, 1995; Hesselbo and Coe, 2000). The Hebrides Basin was, in turn, part of the "Laurasian Seaway", which connected the mid-low latitude Tethys Ocean to the northern high latitude Boreal Ocean (Hesselbo and Coe, 2000; Bjerrum et al., 2001). During the Jurassic, lithofacies and palaeobiogeographic studies suggest there were times when southward-flowing currents (e.g. Boreal down to the Tethys) dominated the seaway, and others when northward currents dominated (summarised in Bjerrum et al., 2001). Broadly, the Jurassic succession on Skye consists of shallow marine siliciclastics and carbonates (Lower Jurassic; Hesselbo et al., 1998) shallowing to lagoonal, deltaic and fluvial in the mid-Middle Jurassic (upper Bajocian; Cox et al., 2002). The Callovian saw a return to marine facies, and the Upper Jurassic sediments (Oxfordian to lowest Kimmeridgian) are dominated by marine mudrocks (Staffin region, Trotternish) or marine siltstone and sandstones (on the Strathaird peninsula; Morton and Hudson, 1995).

On Skye, the emplacement of the Paleocene igneous complex has variably thermally affected all Jurassic sediments older than the Callovian (Thrasher, 1992; Bishop and Abbott, 1995). Callovian to early Kimmeridgian strata with well-preserved fossils occur in outcrop near Staffin Bay, Trotternish, in the northernmost part of the island (Fig. 2). The section at Staffin Bay is renowned for being the most stratigraphically complete Oxfordian section in the UK (Morton and Hudson, 1995; Hesselbo and Coe, 2000), despite the exposure being in fossil coastal landslides (tilted fault blocks). Previous studies have however achieved the reconstruction of a complete composite section (Morton and Hudson, 1995; Hesselbo and Coe, 2000). This area is also the type locality for several of the Boreal middle and upper Oxfordian Zones and Subzones (Sykes & Callomon 1979), which has led to the section being proposed as the Global Stratotype Section and Point (GSSP) for the Oxfordian–Kimmeridgian boundary (Barski et al., 2018).

The regional Cenozoic igneous activity has not affected the shales in this locality (Thrasher, 1992), except very locally where minor igneous intrusions are present (Bishop and Abbot, 1995). Furthermore, the maximum burial depth experienced by the host shales never exceeded 1 km (Morton and Hudson, 1995); Rock Eval data shows the organic matter to be immature (av. T_{max}=424 °C; Nunn, 2009), and biomarker analysis shows exceptional preservation and very low thermal degradation of the organic matter (Lefort et al., 2012). Given (1) that the burial depth did not exceed 1 km, (2) that the igneous activity in the south of the island did not affect Trotternish (Thrasher, 1992), and (3) that the organic matter is not thermally altered (Lefort et al., 2012), we estimate that burial temperatures did not exceed 50 °C in these sediments. It is therefore unlikely that diagenetic alteration or solid-state reordering has affected the numerous belemnites found in this succession, as the calcite must be held at temperatures exceeding 80-120 °C for million year timescales for this to occur (Henkes et al., 2014; Stolper and Eiler 2015). This succession is thus an ideal candidate for a reconstruction of Middle to Late Jurassic temperatures (e.g. Wierzbowski 2004; Nunn et al., 2009). In addition to the pristine preservation of the biogenic calcite and organic matter, there is an excellent biostratigraphic scheme (Sykes & Callomon, 1979; Riding and Thomas, 1997; Hesselbo and Coe, 2000; Barski, 2018 and references therein), supported by Re-Os radioisotope ages (Selby, 2007) and magnetostratigraphy (Przybylski et al., 2010).

The stratigraphy of the Callovian to Kimmeridgian strata at Staffin Bay, Trotternish, consists of the lower Callovian Staffin Bay Formation, the oyster-rich shales of the Upper Ostrea Member, overlain by the conspicuous Belemnite Sands Member, a well-cemented and belemnite-rich siltstone and sandstone bed at the top of the formation (Morton and Hudson, 1995; Hesselbo and Coe, 2000). This formation is overlain by the middle Callovian to lower Kimmeridgian Staffin Shale Formation, which is subdivided into five members. At the base of the formation lies the mid Callovian-aged Dunans Shale Member, which consists of laminated bituminous shales with thin layers of glauconitic silt. It was deposited under largely anoxic conditions, except in the bioturbated glauconitic silts. This is overlain by the well-oxygenated Dunans Clay Member (upper Callovian to Lower Oxfordian), which is composed of bioturbated non-laminated grey-green clays with carbonate nodules (Morton and Hudson, 1995). The formation shallows upward into the uppermost lower to middle Oxfordian Glashvin Silt Member. These dark grey, carbonaceous silts, with occasional beds of green clay, were oxygenated, and this member was still largely deposited below the storm wave base except for occasional large storm events that deposited rare thin sandy layers (Morton and Hudson, 1995). The shallowing trend continues into the paler-coloured and coarser Digg Siltstone Member (middle Oxfordian), where deposition is interpreted to have been occurring close to the fair weather wave base (Morton and Hudson, 1995). There is a facies change at the boundary between pale, fine-grained sandstones with subordinate dark-grey silts of the Digg Siltstone Member and the overlying basal, middle/upper Oxfordian dark glauconitic siltstones of the fossiliferous Flodigarry Shale Member. The Flodigarry Shale Member then grades into dark grey, slightly bituminous shaly clays, where the youngest beds are dated biostratigraphically as latest early Kimmeridgian in age (*cymodoce* zone; Hesselbo and Coe, 2000).

2. Material and methods

2.1 Belemnite selection and preservation

Exceptionally well-preserved belemnite rostrum samples, based on published minor element (Fe concentrations < 20 µg/g, Mn < 12 µg/g) and cathodoluminescence (CL) data (Nunn et al., 2009), were selected for clumped isotope thermometry. These data informed us which samples of rostra calcite were best-preserved overall (e.g. Ullmann et al., 2015), but in order to get an idea of micro-scale variations within a good specimen, and select the best regions for sampling, further analyses were undertaken on a representative subset of those well-preserved samples selected for clumped isotope analyses (Nunn et al., 2009). These samples include one belemnite from each genus (*Cylindroteuthis* and *Pachyteuthis*), and span the oldest, middle and youngest intervals analysed (upper Callovian, mid Oxfordian and lower Kimmeridgian). Micro x-ray fluorescence (µ-XRF), scanning electron microscopy energy dispersive X-ray spectrometry (SEM-EDS), and Electron Backscatter Diffraction (EBSD) mapping of polished belemnite thick sections allowed us to identify the best-preserved regions within the rostra, and assess whether the original biomineralisation crystal patterns are preserved. These methods allow us to assess the preservational state of the selected rostra (taken as representative for all the belemnite rostra analysed for clumped isotopes in this study) from large scale down to very small scale. The µ-XRF analysis were performed at the Natural History Museum of Denmark using an M4-Tornado benchtop µ-XRF. The SEM-EDS and -EBSD analyses were performed at the SEM laboratory at the Geological Survey of Denmark and Greenland (GEUS), which hosts a ZEISS Sigma 300VP Field Emission Scanning Electron Microscope (FE-SEM) that is equipped with 2 Bruker Xflash 6|30 129 eV EDS detectors and a Bruker e-Flash FS EBSD detector. The belemnites were mounted in epoxy resin blocks (40 mm diameter) and, for the sample chosen for EBSD, polished with a final step of 30 minutes polishing with colloidal silica to obtain a scratch-free surface. Only one sample was chosen for EBSD, SK3_5.55. This is considered representative of all samples analysed due to the close likeness observed between it and the other polished specimens under micro-XRF, SEM, and published CL and minor element data (Nunn et al., 2007). Before EBSD analysis, the detector was calibrated based on matching Kikuchi EBSD patterns to ensure results of a high certainty (i.e., certainty >95%).

2.2 Clumped Isotope thermometry

Powdered samples were collected using a dremel drill, away from the apical area and outer edge of the rostrum (except instances where we specifically wished to measure an altered part of the rostrum for comparative purposes), with samples spanning many growth lines. The tip of the rostrum was avoided. Clumped isotope measurements were carried out at the ETH Zurich using a ThermoFisher Scientific MAT253 mass spectrometer coupled to a Kiel IV carbonate preparation device, following the methods described in Müller et al. (2017). The Kiel IV device included a PoraPakQ trap kept at -40 °C to eliminate potential organic contaminants. Samples were measured between November 2018 and July 2019 by measuring maximum 2 replicates of each sample per measuring session which consists generally of 24 samples of 130-150 µg interspersed with 20 replicates of each of the three carbonate standards ETH-1, ETH-2 and ETH-3 (Bernasconi et al., 2018). The samples were analysed in LIDI mode with 400 seconds of integration of sample and reference gas. The calculations and corrections were done with the software Easotope (John & Bowen, 2016) using the revised "Brand parameters" for ^{17}O correction as suggested by Daëron et al. (2016). The data are reported with respect to the carbon dioxide equilibration scale CDES. Temperatures were calculated using the Kele et al. (2015) calibration recalculated with the "Brand parameters" and the new accepted values for the ETH standards as reported in Bernasconi et al. (2018). These were chosen because calibration and samples were measured and converted to the absolute reference frame with the same methodology as in ETH set-up. Furthermore, this revised Kele (2015) calibration is statistically indistinguishable from independent calibrations for marine biogenic calcite from other laboratories (Peral et al. 2018, Meinicke et al. 2020; Breitenbach et al. 2018), suggesting that it is appropriate for marine biogenic carbonates.

3. Results

The preservation of all analysed belemnites is exceptional, as shown by the micro-XRF and EDS element mapping of polished belemnite blocks (see Figs. 3, 4 and Appendix B), and is supported by the previously published minor element and CL data (Nunn et al., 2009). EBSD maps of selected belemnites further demonstrate the near-pristine preservation state, with no diagenetic recrystallisation of the calcite, except in the apical or outer rim areas. The EBSD map area of belemnite SK3_5.55 covers a well-preserved section of the rostrum with well-preserved calcite and a distinct hollow alveolar area that is infilled with a fine-grained carbonate-rich cement (Fig. 3A). The SEM-BSE image (Fig. 3B) and EBSD data (Fig. 3) show radiaxial fibrous calcites that increase in size (length and width) from the centre towards the outer rim, in agreement with published SEM and light-microscopy observations on very well-preserved belemnite rostra (Ullmann et al., 2015; Benito at al., 2016). The c-axes in the lamellae are similar in orientation but show rotation along the crystallographic c-axis resulting in a rotating a-axis (Fig. 3F). Each of the radial lamellae has a slight bend of 10 – 15 degrees, as indicated by the broad band of the stereographic projection of the calcite crystals (Fig. 3D). This observation confirms the postulation presented in Ullmann et al (2015) that the crystallographic orientation should change close to the apical line/alveolar cavity. The observed lamellae are a primary biomineralisation fabric, as recrystallized crystals are expected to be not elongated but more equant in size and erratic in orientation (e.g. Casella et al., 2018).

In the growth rings in the apical area the SEM-EDS elemental maps reveal compositional changes in Mg and S, but not in Fe and Mn (Fig. 4). Enrichment of Mg in the apical area is believed to be related to distortion of the calcite crystals close to the apical line, whereas beyond the apical area variations in Mg may be related to calcite precipitation rates, with higher calcification rates leading to incorporation of less Mg (Ullmann et al., 2015; Ullmann and Pogge von Strandmann 2017). This may be the same case for S, as these two elements co-vary (Fig. 4 and Appendix B). The fact that Mn and Fe show enrichment in different areas (opposite trend to Mg and S; Fig. 4) supports the conclusion that variations in Mg and S are primary (biomineralisation) phenomena and not related to diagenesis.

The Δ_{47} values range between 0.650(±0.0026) ‰ and 0.695(±0.023) ‰. The standard deviation for the clumped isotope measurements, calculated from ≥ 10 replicate analyses are between 0.017 ‰ and 0.049 ‰ (mean 0.029 ‰). The Δ_{47} values yield seawater temperatures ranging between 19°C and 32 °C, with a median temperature of 26 °C. While excluding the apical line calcite measurements (this area of the belemnite is notoriously known to favour the precipitation of early diagenetic calcite, e.g. Ullmann et al., 2015; Benito et al., 2016), the range is narrowed to 21 – 32 °C, with the mean and median remaining at 26 °C. The average uncertainty calculated from the 95 % confidence level for the reconstructed temperatures is ±5 °C. *Pachyteuthis* are consistently within error of the *Cylindroteuthis* data, and the differences in Δ_{47} between the two genera are not statistically significant at the 2σ level.

The $\delta^{18}O_{sw}$ values were calculated by inputting the reconstructed clumped isotope temperatures into the various published oxygen isotope thermometry equations for different calcite types, both organic and inorganic (e.g. Epstein et al., 1953; Shackleton, 1974; Anderson and Arthur, 1983; Kim and O'Neil,. 1997; Coplen, 2007; Brand et al., 2013; see Appendix A). The majority of these equations returned similar $\delta^{18}O_{sw}$ values to the Kim and O'Neil (1997) equation derived for inorganic calcite. Only the equations for equilibrium inorganic calcites of, Coplen, 2007; Kele et al. (2015), and Daëron (2019) yielded significantly lower $\delta^{18}O_{sw}$ (Fig. 5).

4. Discussion

4.1 Belemnite preservation and life habits

As demonstrated by our multi-proxy, thorough investigation of the belemnite calcite, the preservation of the belemnites is exceptional, with the sampled areas showing no recrystallisation. However, recent geochemical and electron beam work on the ultrastructure of well-preserved belemnites has identified the existence of two distinct calcite phases within the rostrum, for belemnites from the Middle Jurassic and younger (Benito et al., 2016; Hoffmann et al., 2016). The origin of one ultrastructural element which forms units of roughly tetrahedral shape that point away from the apical line is considered primary, i.e. secreted actively by the belemnite (Hoffmann et al., 2016).

The interpretation of the second ultrastructure filling the remaining fraction of the rostrum is more uncertain. It has previously been suggested that this second phase is an early diagenetic cement, and that the belemnite rostrum in fact had a porosity of 50 – 90 % (e.g. Benito et al., 2016; Hoffmann et al., 2016). This interpretation, however, is contradicted by geochemical evidence documenting that the isotopic and chemical composition of the second phase is incompatible with diagenetic cements (e.g., Price et al., 2015; Stevens et al., 2017). Clear geochemical trends relating to precipitation rate and isotopic signatures that can be matched through multiple profiles through the same rostrum

(Ullmann et al., 2015; Ullmann and Pogge von Strandmann 2017) contradict the notion that variable amounts of diagenetic cement would have filled an originally highly porous structure.

In order to understand the meaning of belemnite temperature measurements and consequently paleoecology and palaeoenvironmental signatures, it is of some importance to determine confidently the timing of biomineral formation. If the second calcite phase were formed at the seafloor during earliest diagenesis, a bias toward colder temperatures would be expected if the studied taxa generally occupied the upper part of the water column. Our data, however, support the hypothesis that this second phase – if present – is also formed during the animal's life and would unlikely have formed only during times when the belemnite dwelled at the seafloor. The temperatures derived from our clumped isotope measurements are at the upper end of the expected range for belemnites (e.g. 10 – 30 °C, Hoffmann and Stevens, 2019), and sub-samples from the visibly porous apical area yield colder temperatures than samples taken from the intermediate growth increments (between apical line and rim; Table 1; Fig. 5). This originally slightly porous area (Ullmann et al., 2015) is prone to diagenetic alteration, as indicated by the higher concentrations of Mn and Fe in this region (Fig. 4 and Appendix B), thus favouring the circulation of diagenetic fluids (e.g. Ullmann et al., 2015; Benito et al., 2016). The observed diagenetic precipitation most likely occurred at an early stage at the seafloor, prior to burial, or within the uppermost metre of the sediment, which is generally well mixed by bioturbation and whose pore-water remains in equilibrium with seawater. In both cases, this diagenetic calcite would reflect bottom water temperatures, which would explain the lower temperatures obtained in the apical line as compared to other areas of the rostrum. Consequently, formation of the second calcite phase is incompatible with a bias towards bottom water temperatures in the bulk of the rostrum as this process should have led to similar temperature bias as in the apical zone. On the basis of our data it appears much more likely that the formation of the second calcite phase is (nearly) simultaneous with the formation of the first phase, and secretion is continuous.

The reconstructed clumped isotope temperatures are > 10 °C warmer than those estimated by Nunn (2009) using oxygen isotope thermometry from the same samples (12 °C average vs 26 °C average), with an assumed $\delta^{18}O_{sw}$ of -1 ‰ (Fig. 5). This is also much warmer than temperatures estimated by Wierzbowski (2004) using oxygen isotope thermometry on belemnites from the same section (Staffin Bay). These clumped isotope temperatures therefore support the interpretation that Middle–Late Jurassic belemnite habitats, at least for the two genera examined here, were pelagic, i.e. within the upper 200 m of the water column (e.g. in the photic zone, Klug et al., 2016; Vickers et al., 2019; Hoffmann and Stevens, 2019). This is further supported by the lower temperatures obtained from the calcite of the apical line which most likely reflect bottom-water temperatures, as compared to temperatures obtained from other areas of the rostrum (Table 1). This is contrary to older studies which have suggested that *Cylindroteuthis* and *Pachyteuthis* were nektobenthic, based on oxygen isotope measurements and rostrum morphology (e.g. Matrill et al., 1994; Mutterlose et al., 2010). There was no significant difference in the measured temperatures between *Cylindroteuthis* and *Pachyteuthis* samples, given the average uncertainty of ±5 °C (Fig. 5), which suggests that they inhabited similar, environments, although it is possible that one genus may have favoured slightly colder waters/deeper depths that were within this confidence interval. However, the lack of significant statistical difference between the two genera in the large ^{18}O dataset of Nunn et al. (2009), and the fact they are found together in the sediments, supports the former conclusion.

4.2 Seawater temperature and $\delta^{18}O$ reconstruction

In modern oceans, whilst the global average deep water $\delta^{18}O_{sw}$ is 0 ‰ SMOW, there are very few places in the surface ocean that actually have a $\delta^{18}O_{sw}$ of 0 ‰ (e.g. LeGrande and Schmidt, 2006) with a general trend of higher values in the tropics decreasing towards high latitudes. The $\delta^{18}O_{sw}$ is variable with depth and geography, and the local $\delta^{18}O_{sw}$ is dependent on the relative contributions of meteoric water and evaporation. Whilst there are uncertainties in local palaeogeography and palaeoceanography, GCM models for the Mesozoic return a large spread from very light values (e.g. as low as -7 ‰) for the semi-enclosed Boreal Ocean, and relatively heavy values (e.g. 0 to 0.5 ‰) for the Tethys ocean in an ice-free world (Zhou et al., 2008, Cretaceous simulation). In the present study, reconstructed $\delta^{18}O_{sw}$ values, using most of the common calcite-thermometry equations (e.g. Kim and O'Neil, 1997, for inorganic calcite; Brand et al., 2013, for brachiopod calcite; Shackleton, 1974, for benthic foraminifera; Epstein et al., 1953, and Anderson and Arthur, 1983, for molluscan calcite) are surprisingly high, up to as much as +3 ‰ (Fig. 5). This is approximately 1 ‰ heavier than may be expected for even the evaporative middle part of the North Atlantic today (e.g. Schmidt et al., 1999; LeGrande and Schmidt, 2006), and indeed, such high values are not seen in sea water anywhere today except in hypersaline brines or entirely continental water bodies (Schmidt et al., 1999). For a greenhouse Earth, with global average $\delta^{18}O_{sw}$ of -1 ‰ (Shackleton and Kennett, 1975), this high value is even more unlikely in any ocean-connected basin (e.g. Zhou et al., 2008), and indeed, there is no sedimentological or palaeontological evidence for hypersalinity in the basin (e.g. Morton and Hudson, 1995; Hesselbo and Coe, 2000; Lefort et al., 2012). Only the equations of Coplen (2007) and Daëron et al., (2019), both calibrated for slow-growing terrestrial vein calcite; and Kele et al. (2015) for travertine calcite, provide $\delta^{18}O_{sw}$ values that range under normal conditions in a semi-enclosed to open basin (Fig. 5). This finding is in concert with recent results from other Mesozoic belemnite clumped isotope studies (e.g. Price and Passey, 2013; Wierzbowski et al., 2018: Price et al., 2019; Vickers et al., 2019).

The reason for why these equations fit better may be that many of the more traditional calcite thermometry equations do not in fact represent true equilibrium fractionation between calcite and water, as has been recently demonstrated by Daëron et al. (2019). These authors showed that true equilibrium calcite-water fractionation values are systematically c. 1.5 ‰ greater than in the (biotic and abiotic) calcites used to derive the more common thermometry equations (e.g. Epstein et al., 1953; Anderson and Arthur, 1983; Kim and O'Neil, 1997 etc.). Our findings show that the equations of Coplen, 2007; Kele et al. (2015), and Daëron et al. (2019), for extremely slow-growing, abiotic calcites, when applied to well-preserved belemnite calcite, return $\delta^{18}O_{sw}$ values within the expected range for open water to semi-enclosed basin setting (-2 to +1 ‰; Fig. 5). Whilst the biomineralisation in belemnites is very different to slow-growing, abiotic precipitates (belemnites are believed to be have had a lifespan of 1 – 2 years, Hoffmann and Stevens, 2019), this study supports the evidence that they precipitated their rostrum in near-equilibrium with ambient seawater. This finding agrees with evidence that modern coleoids biomineralise in near-equilibrium with the ambient seawater (Rexfort and Mutterlose, 2006; Price et al., 2009).

4.3 Palaeogeographic implications

The average temperature (26 °C) is slightly warmer than that derived by Δ_{47} on belemnites from the Middle Russian Sea (23 °C, Fig. 6), which may indicate more of an Arctic water source for the Middle Russian Sea vs. a Tethyan source for the Hebrides Basin, or may be a result of some visually-imperceptive solid-state re-ordering in the belemnite calcite. Nonetheless, despite uncertainties as to the absolute temperature and reconstructed $\delta^{18}O_{sw}$ values, trends in both may shed light on changes in circulation patterns in the narrow Laurasian Seaway. There is uncertainty in the main direction of the flow of dominating currents in the Laurasian Seaway through time, which could either be at times southward (Boreal-sourced) or northward (Tethyan-sourced; Bjerrum et al., 2001; Dera et al., 2015). Temperatures in the Hebrides Basin average around 24 °C in the Callovian to lowest Oxfordian, increasing in the middle Oxfordian to 27 °C, and remain high (av. 29 °C) in the Upper Oxfordian and lowest Kimmeridgian (*baylei* zone; Fig. 6). In the Lower Kimmeridgian *cymodoce* zone there is an apparent shift to lower temperatures (22 °C), a change in temperature that is greater than the ± 5 °C uncertainty in the measurements (Fig. 6).

Temperature trends in the southern North Sea (Euro-Boreal realm, Fig. 1), reconstructed using sporomorph data (Abbink et al., 2001), support the Skye belemnite clumped isotope record during the Callovian and Oxfordian, with cool temperatures in the Upper Callovian, and significant warming in the middle Oxfordian (Fig. 6). Our results contrast to the belemnite clumped isotope temperature record from the Russian Platform through the same interval (Wierzbowski et al., 2018), which shows a mid-Oxfordian cooling trend (Fig. 6).

There is an observable isotopic gradient, from very low (unradiogenic) $\varepsilon Nd_{(t)}$ values in the Arctic regions to higher (more radiogenic) values in the Tethyan open marine domains (Dera et al., 2015), and the $\varepsilon Nd_{(t)}$ records from the Euro-Boreal Realm and the Russian platform are quite different in the Callovian to mid-Oxfordian (c. 2 ε-units more positive in the Russia Platform). A clear rise observed in $\varepsilon Nd_{(t)}$ in the Euro-Boreal (and peri-Tethyan) areas during the mid-Oxfordian is not apparent in the Russian Platform data (Dera et al., 2015). This rise in $\varepsilon Nd_{(t)}$ has been attributed to a strengthening of southern Tethyan surface currents intruding the northern domains (Dera et al., 2015), which, though $\varepsilon Nd_{(t)}$ data for the Hebrides Basin are lacking, may explain the shift to warmer values in the Skye belemnite clumped temperatures in the Middle Oxfordian.

The shift to cooler temperatures in the early Kimmeridgian is suggested in the Russian Platform dataset, and is not clear in the southern North Sea (terrestrial) sporomorph record (Abbink et al., 2001; Fig. 6). Reconstructed $\delta^{18}O_{sw}$ in both the Russian Platform and the Hebrides Basin show a marked decrease here. Published $\varepsilon Nd_{(t)}$ data show closer agreement between Euro-Boreal and Peri-Tethyan realms and the Russian Platform than in earlier times, and all three show a decrease in $\varepsilon Nd_{(t)}$ in the Late Oxfordian to very unradiogenic (Boreal water) values. The clumped isotope data therefore support the interpretation that a change in ocean circulation may have driven this Kimmeridgian cooling trend, by strengthening the influx of Boreal waters down the Viking Corridor, and weakening the Tethyan influence (Fig. 1). This may account for the lowering of $\varepsilon Nd_{(t)}$ values in the Russian Platform and Euro-Boreal realms (Dera et al., 2015) and the cooling and freshening of the Russian platform and Hebrides Basin (Wierzbowski et al., 2018) and this is documented by the present study. This interpretation is also supported by observed changes in marine fauna – e.g. the southward migrations of boreal ammonites, and regional retreats of coral reefs (Dera et al., 2015).

5. Conclusions

Our clumped isotope dataset from exceptionally well-preserved belemnites from Staffin Bay, Isle of Skye reveals that seawater temperatures throughout the Callovian to Early Kimmeridgian were significantly warmer than previously supposed by conventional oxygen isotope thermometry. These data support the view that belemnites, at least those of the genera *Cylindroteuthis* and *Pachyteuthis*, inhabited the upper 200 m of the water column, and were nektonic rather than nektobenthic. These temperature and $\delta^{18}O_{sw}$ estimates demonstrate that slow-growing, abiotic calcite thermometry equations are more applicable to belemnite calcite in conventional stable isotope studies, and indicate that $\delta^{18}O_{sw}$ may have varied significantly in the Hebrides Basin throughout this interval.

Trends in the belemnite clumped isotope temperatures and in the reconstructed $\delta^{18}O_{sw}$ reveal changes in palaeocurrent in the Laurasian Seaway throughout the Callovian-Kimmeridgian and, when considered with other published temperature and $\varepsilon Nd_{(t)}$ studies, support the following conclusions:

1) Observed mid-Callovian warming was due to a strengthening of the northward-flowing, warm, saline Tethyan current into the Euro-Boreal Realm and Laurasian Seaway, but not onto the Russian Platform.

2) The southward flowing, cold, fresher Boreal current strengthened down the Viking Corridor and Mezen-Pechora strait in the Early Kimmeridgian, resulting in cooler waters entering the Laurasian Seaway (Hebrides Basin), and Russian Platform, but did not extend as far south as the southern North Sea.

Acknowledgements

Funding for this study was gratefully received from the Danish Council for Independent Research–Natural Sciences grant DFF - 7014-00142 to C. Korte and Swiss SNF (project 200021_169849) to S. Bernasconi, and a UK Natural Environment Research Council (NERC) grant (NE/J020842/1) to G.D. Price. S. Hesselbo and C. Ullmann acknowledge funding from the UK Natural Environment Research Council (NE/N018508/1). We are very grateful to Daniel Kim Peel Wielandt and Quadlab for running the μ-XRF analysis for us, funded by the Villum Foundation. We would like to thank Madalina Jaggi at ETH Zurich for running the clumped isotope analyses on the belemnites.

References

Abbink, O., Targarona, J., Brinkhuis, H., Visscher, H., 2001. Late Jurassic to earliest Cretaceous palaeoclimatic evolution of the southern North Sea. Global and Planetary Change 30, 231-256.

Anderson, T.F., Arthur, M.A., 1983. Stable isotopes of oxygen and carbon and their application to sedimentologic and environmental problems, in: Stable Isotopes in Sedimentary Geology, Arthur, M.A., Anderson, T.F., Kaplan, I.R., Veizer, J., Land, L. S. (Eds), Society of Economic Palaeontologists and Mineralogists Short course, Tulsa, Oklahoma, 10, 1.1–1–151.

Bailey, T., Rosenthal, Y., McArthur, J., Van de Schootbrugge, B., Thirlwall, M., 2003. Paleoceanographic changes of the Late Pliensbachian–Early Toarcian interval: a possible link to the genesis of an Oceanic Anoxic Event. Earth and Planetary Science Letters 212, 307-320.

Barski, M., 2018. Dinoflagellate cyst assemblages across the Oxfordian/Kimmeridgian boundary (Upper Jurassic) at Flodigarry, Staffin Bay, Isle of Skye, Scotland–a proposed GSSP for the base of the Kimmeridgian. Volumina Jurassica 16, 51-62.

Benito, M.I., Reolid, M., Viedma, C., 2016. On the microstructure, growth pattern and original porosity of belemnite rostra: insights from calcitic Jurassic belemnites. Journal of Iberian Geology 42, 201.

Bernasconi, S.M., Müller, I.A., Bergmann, K.D., Breitenbach, S.F., Fernandez, A., Hodell, D.A., Jaggi, M., Meckler, A.N., Millan, I., Ziegler, M., 2018. Reducing uncertainties in carbonate clumped isotope analysis through consistent carbonate-based standardization. Geochemistry, Geophysics, Geosystems 19, 2895-2914.

Berner, R.A., Kothavala, Z., 2001. GEOCARB III: A revised model of atmospheric CO2 over Phanerozoic time. American Journal of Science 301, 182-204.

Bishop, A., Abbott, G., 1995. Vitrinite reflectance and molecular geochemistry of Jurassic sediments: the influence of heating by Tertiary dykes (northwest Scotland). Organic Geochemistry 22, 165-177.

Bjerrum, C.J., Surlyk, F., Callomon, J.H., Slingerland, R.L., 2001. Numerical paleoceanographic study of the Early Jurassic transcontinental Laurasian Seaway. Paleoceanography 16, 390-404.

Brand, U., Azmy, K., Bitner, M., Logan, A., Zuschin, M., Came, R., Ruggiero, E., 2013. Oxygen isotopes and MgCO3 in brachiopod calcite and a new paleotemperature equation. Chemical Geology 359, 23-31.

Brassell, S.C., G. Eglinton, I.T. Marlowe, U. Pflaumann, and M. Sarnthein, Molecular stratigraphy: A new tool for climatic assessment, Nature, 320, 129-133, 1986.Callomon, J.H., 2003. The Middle Jurassic of western and northern Europe: its subdivisions, geochronology and correlations. Geological Survey of Denmark and Greenland Bulletin 1, 61-73.

Breitenbach, S.F., Mleneck-Vautravers, M.J., Grauel, A.L., Lo, L., Bernasconi, S.M., Müller, I.A., Rolfe, J., Gázquez, F., Greaves, M. and Hodell, D.A., 2018. Coupled Mg/Ca and clumped isotope analyses of foraminifera provide consistent water temperatures. Geochimica et Cosmochimica Acta, 236, pp.283-296.

Came, R.E., Eiler, J.M., Veizer, J., Azmy, K., Brand, U., Weidman, C.R., 2007. Coupling of surface temperatures and atmospheric CO_2 concentrations during the Palaeozoic era. Nature 449, 198.

Casella, L.A., Griesshaber, E., Roda, M.S., Ziegler, A., Mavromatis, V., Henkel, D., Laudien, J., Häussermann, V., Neuser, R.D., Angiolini, L. and Dietzel, M., 2018. Micro-and nanostructures reflect the degree of diagenetic alteration in modern and fossil brachiopod shell calcite: A multi-analytical screening approach (CL, FE-SEM, AFM, EBSD). Palaeogeography, Palaeoclimatology, Palaeoecology, 502, 13-30.

Coplen, T.B., 2007. Calibration of the calcite–water oxygen-isotope geothermometer at Devils Hole, Nevada, a natural laboratory. Geochimica et Cosmochimica Acta 71, 3948-3957.

Cox, B., Page, K., Morton, N., 2002. The Middle Jurassic stratigraphy of Scotland, in: Cox, B., Sumbler (Eds.), British Middle Jurassic Stratigtraphy. Geological Conservation Review Series. Joint Nature Conservation Committee, Peterborough, 363-372.

Daëron, M., Blamart, D., Peral, M., Affek, H., 2016. Absolute isotopic abundance ratios and the accuracy of Δ_{47} measurements. Chemical Geology 442, 83-96.

Daëron, M., Drysdale, R.N., Peral, M., Huyghe, D., Blamart, D., Coplen, T.B., Lartaud, F. and Zanchetta, G., 2019. Most Earth-surface calcites precipitate out of isotopic equilibrium. Nature Communications, 10, 1-7.

de Bar, M. W., Rampen, S. W., Hopmans, E. C., Damsté, J. S. S. & Schouten, S. Constraining the applicability of organic paleotemperature proxies for the last 90 Myrs. Organic geochemistry 128, 122-136 (2019).

Dera, G., Prunier, J., Smith, P.L., Haggart, J.W., Popov, E., Guzhov, A., Rogov, M., Delsate, D., Thies, D., Cuny, G., 2015. Nd isotope constraints on ocean circulation, paleoclimate, and continental drainage during the Jurassic breakup of Pangea. Gondwana Research 27, 1599-1615.

Eiler, J.M., 2007. “Clumped-isotope” geochemistry—The study of naturally-occurring, multiply-substituted isotopologues. Earth and Planetary Science Letters 262, 309-327.

Epstein, S., Buchsbaum, R., Lowenstam, H.A., Urey, H.C., 1953. Revised carbonate-water isotopic temperature scale. Geological Society of America Bulletin 64, 1315-1326.

Henkes, G.A., Passey, B.H., Grossman, E.L., Shenton, B.J., Pérez-Huerta, A., Yancey, T.E., 2014. Temperature limits for preservation of primary calcite clumped isotope paleotemperatures. Geochimica et cosmochimica acta 139, 362-382.

Hesselbo, S.P., Coe, A.L., 2000. Jurassic sequences of the Hebrides Basin, Isle of Skye, Scotland. In: Graham, J.R. & Ryan, A. (eds) Field Trip Guide Book, International Sedimentologists Association Meeting, Dublin. University of Dublin, Dublin, 41–58.

Hesselbo, S.P., Jenkyns, H.C., 1998. British lower Jurassic sequence stratigraphy. Mesozoic and Cenozoic Sequence Stratigraphy of European Basins, SEPM Special Publications No. 60.

Hewitt, R.A., 2000. Geological interpretations from cephalopod habitat and implosion depth limits. Revue de paléobiologie, 8, pp.95-107.

Hoffmann, R., Richter, D.K., Neuser, R.D., Jöns, N., Linzmeier, B.J., Lemanis, R.E., Fusseis, F., Xiao, X. and Immenhauser, A., 2016. Evidence for a composite organic–inorganic fabric of belemnite rostra: Implications for palaeoceanography and palaeoecology. Sedimentary Geology, 341, pp.203-215.

Hoffmann, R. and Stevens, K., 2019. The palaeobiology of belemnites–foundation for the interpretation of rostrum geochemistry. Biological Reviews, 95, pp.94-123.

John, C.M., Bowen, D., 2016. Community software for challenging isotope analysis: First applications of 'Easotope'to clumped isotopes. Rapid Communications in Mass Spectrometry 30, 2285-2300.

Kele, S., Breitenbach, S.F., Capezzuoli, E., Meckler, A.N., Ziegler, M., Millan, I.M., Kluge, T., Deák, J., Hanselmann, K., John, C.M., 2015. Temperature dependence of oxygen-and clumped isotope fractionation in carbonates: a study of travertines and tufas in the 6–95 C temperature range. Geochimica et Cosmochimica Acta 168, 172-192.

Kim, S.-T., O'Neil, J.R., 1997. Equilibrium and nonequilibrium oxygen isotope effects in synthetic carbonates. Geochimica et Cosmochimica Acta 61, 3461-3475.

Klug, C., Schweigert, G., Fuchs, D., Kruta, I., Tischlinger, H., 2016. Adaptations to squid-style high-speed swimming in Jurassic belemnitids. Biology letters 12, 20150877.

Korte, C., Hesselbo, S.P., Ullmann, C.V., Dietl, G., Ruhl, M., Schweigert, G., Thibault, N., 2015. Jurassic climate mode governed by ocean gateway. Nature communications 6, 10015.

Lefort, A., Hautevelle, Y., Lathuilière, B., Huault, V., 2012. Molecular organic geochemistry of a proposed stratotype for the Oxfordian/Kimmeridgian boundary (Isle of Skye, Scotland). Geological Magazine 149, 857-874.

LeGrande, A.N., Schmidt, G.A., 2006. Global gridded data set of the oxygen isotopic composition in seawater. Geophysical Research Letters 33.

Martill, D.M., Taylor, M.A., Duff, K.L., Riding, J.B. and Bown, P.R., 1994. The trophic structure of the biota of the Peterborough Member, Oxford Clay Formation (Jurassic), UK. Journal of the Geological Society, 151(1), pp.173-194.

Meinicke, N., Ho, S.L., Hannisdal, B., Nürnberg, D., Tripati, A., Schiebel, R. and Meckler, A.N., 2020. A robust calibration of the clumped isotopes to temperature relationship for foraminifers. Geochimica et Cosmochimica Acta, 270, pp.160-183.

Morton, N., Hudson, J.D., 1995. Field guide to the Jurassic of the isles of Raasay and Skye, Inner Hebrides, NW Scotland, in: Taylor, P. (Ed.), Field geology of the British Jurassic. Geological Society, London, London, pp. 209 - 280.

Müller, I.A., Fernandez, A., Radke, J., Van Dijk, J., Bowen, D., Schwieters, J., Bernasconi, S.M., 2017. Carbonate clumped isotope analyses with the long-integration dual-inlet (LIDI) workflow: Scratching at the lower sample weight boundaries. Rapid Communications in Mass Spectrometry 31, 1057-1066.

Mutterlose, J., Malkoc, M., Schouten, S., Sinninghe Damsté, J.S., Forster, A., 2010. TEX_{86} and stable $\delta^{18}O$ paleothermometry of early Cretaceous sediments: Implications for belemnite ecology and paleotemperature proxy application. Earth and Planetary Science Letters 298, 286-298.

Nunn, E.V., Price, G.D., Hart, M.B., Page, K.N., Leng, M.J., 2009. Isotopic signals from Callovian–Kimmeridgian (Middle–Upper Jurassic) belemnites and bulk organic carbon, Staffin Bay, Isle of Skye, Scotland. Journal of the Geological Society 166, 633-641.

Peral, M., Daëron, M., Blamart, D., Bassinot, F., Dewilde, F., Smialkowski, N., Isguder, G., Bonnin, J., Jorissen, F., Kissel, C. and Michel, E., 2018. Updated calibration of the clumped isotope thermometer in planktonic and benthic foraminifera. Geochimica et Cosmochimica Acta, 239, pp.1-16.

Podlaha, O.G., Mutterlose, J., Veizer, J., 1998. Preservation of delta 18 O and delta 13 C in belemnite rostra from the Jurassic/Early Cretaceous successions. American Journal of Science 298, 324-347.

Price, G.D., Hart, M.B., Wilby, P.R., Page, K.N., 2015. Isotopic analysis of Jurassic (Callovian) mollusks from the Christian Malford Lagerstätte (UK): Implications for ocean water temperature estimates based on belemnoids. Palaios 30, 645-654.

Price, G.D., Passey, B.H., 2013. Dynamic polar climates in a greenhouse world: Evidence from clumped isotope thermometry of Early Cretaceous belemnites. Geology 41, 923-926.

Price, G.D., Twitchett, R.J., Smale, C. and Marks, V., 2009. Isotopic analysis of the life history of the enigmatic squid Spirula spirula, with implications for studies of fossil cephalopods. Palaios, 24(5), pp.273-279.

Przybylski, P.A., Ogg, J.G., Wierzbowski, A., Coe, A.L., Hounslow, M.W., Wright, J.K., Atrops, F., Settles, E., 2010. Magnetostratigraphic correlation of the Oxfordian–Kimmeridgian boundary. Earth and Planetary Science Letters 289, 256-272.

Rexfort, A. and Mutterlose, J., 2006. Stable isotope records from Sepia officinalis—a key to understanding the ecology of belemnites?. *Earth and Planetary Science Letters*, *247*(3-4), pp.212-221.

Riding, J.B., Thomas, J.E., 1997. Marine palynomorphs from the Staffin Bay and Staffin Shale formations (Middle-Upper Jurassic) of the Trotternish Peninsula, NW Skye. Scottish Journal of Geology 33, 59-74.

Schmidt, G.A., G. R. Bigg and E. J. Rohling. 1999. "Global Seawater Oxygen-18 Database - v1.22" https://data.giss.nasa.gov/o18data/

Selby, D., 2007. Direct Rhenium-Osmium age of the Oxfordian-Kimmeridgian boundary, Staffin bay, Isle of Skye, UK, and the Late Jurassic time scale. Norwegian Journal of Geology/Norsk Geologisk Forening 87.

Shackleton, N., 1974. Attainment of isotopic equilibrium between ocean water and the benthonic foraminifera genus Uvigerina: isotopic changes in the ocean during the last glacial.

Shackleton, N., Kennett, J., 1975. Paleotemperature history of the Cenozoic and the initiation of Antarctic glaciation: oxygen and carbon isotope analyses in DSDP Sites 277, 279, and 281. US Government Printing Office, Washington DC.

Stevens, K., Griesshaber, E., Schmahl, W., Casella, L.A., Iba, Y., Mutterlose, J., 2017. Belemnite biomineralization, development, and geochemistry: The complex rostrum of Neohibolites minimus. Palaeogeography, palaeoclimatology, palaeoecology 468, 388-402.

Stolper, D.A., Eiler, J.M., 2015. The kinetics of solid-state isotope-exchange reactions for clumped isotopes: A study of inorganic calcites and apatites from natural and experimental samples. American Journal of Science 315, 363-411.

Sykes, R.M., Callomon, J.H., 1979. The Amoeboceras zonation of the Boreal upper Oxfordian. Palaeontology 22, 839-903.

Thrasher, J., 1992. Thermal effect of the Tertiary Cuillins Intrusive Complex in the Jurassic of the Hebrides: an organic geochemical study. Geological Society, London, Special Publications 62, 35-49.

Ullmann, C.V. and Pogge von Strandmann, P.A., 2017. The effect of shell secretion rate on Mg/Ca and Sr/Ca ratios in biogenic calcite as observed in a belemnite rostrum. Biogeosciences, 14, pp.89-97.

Ullmann, C., Frei, R., Korte, C., Hesselbo, S.P., 2015. Chemical and isotopic architecture of the belemnite rostrum. Geochimica et Cosmochimica Acta 159, 231-243.

Vickers, M.L., Bajnai, D., Price, G.D., Linckens, J., Fiebig, J., 2019. Southern high-latitude warmth during the Jurassic–Cretaceous: New evidence from clumped isotope thermometry. Geology.

Voigt, S., Wilmsen, M., Mortimore, R., Voigt, T., 2003. Cenomanian palaeotemperatures derived from the oxygen isotopic composition of brachiopods and belemnites: evaluation of Cretaceous palaeotemperature proxies. International Journal of Earth Sciences 92, 285-299.

Wierzbowski, A., Coe, A.L., Hounslow, M.W., MATYJA, B.A., Ogg, J.G., Page, K.N., Wierzbowski, H., Wright, J.K., 2006. A potential stratotype for the Oxfordian/Kimmeridgian boundary: Staffin Bay, Isle of Skye, UK. Volumina Jurassica 4, 17-33.

Wierzbowski, H., 2004. Carbon and oxygen isotope composition of Oxfordian–Early Kimmeridgian belemnite rostra: palaeoenvironmental implications for Late Jurassic seas. Palaeogeography, Palaeoclimatology, Palaeoecology 203, 153-168.

Wierzbowski, H., Bajnai, D., Wacker, U., Rogov, M.A., Fiebig, J., Tesakova, E.M., 2018. Clumped isotope record of salinity variations in the Subboreal Province at the Middle–Late Jurassic transition. Global and planetary change.

Zhou, J., Poulsen, C., Pollard, D., White, T., 2008. Simulation of modern and middle Cretaceous marine $\delta^{18}O$ with an ocean-atmosphere general circulation model. Paleoceanography 23, PA3223.

TABLES AND FIGURES

Table 1: Summary of the samples analysed and clumped isotope data from the Staffin Bay Section, as presented in this study. Full details, including the published trace element data (Nunn et al., 2007) can be found in Appendix A. Detailed images from the EDS, BSE and μ-XRF analyses can be found in Appendix B.

Figure 1: Palaeogeographic reconstruction showing the situation of Isle of Skye, the Laurasian Seaway (red outline) and other regions discussed in the text during the Jurassic. (Map modified after Dera et al., 2015).

Figure 2: **(A)** Map of Scotland showing location of Isle of Skye (in red) and Staffin Bay (rectangle). **(B)** Staffin Bay with sampling localities marked.

Figure 3: (A) Photograph of the belemnite SK3_5.55. Scale bar is 1 cm. B) SEM-BSE micrograph of the analysed area shown in A. **(C)** Kikuchi EBSD pattern calibration result of 95.2% certainty. **(D)** Maps of EBSD crystallographic orientations along the x, y, and z axes, as well as a grain map that delineates individual grains with distinct crystallographic orientations. **(E)** Stereographic projections of the poles to the crystal faces. Calcite stereographic projections measured at 153027 points (56.7%), 28066 zero solutions (10.4%). **(F)** Line scan across the calcite lamellae indicating rotation around the crystallographic c-axis of roughly 60 degrees. **(G)** Zoomed in IPFY map, schematic illustrating the rotation of the calcite crystals, and stereographic projections of the poles to the crystal faces.

Figure 4: (A) Photograph of the belemnite SK4_0.2. White square indicates where insets (B) to (F) are taken from**. (B)** SEM secondary electron photomicrograph of area chosen for EDS element maps **(C) - (F)** EDS element maps for Mg, S, Mn and Fe.

Figure 5: Measured clumped isotope temperatures from selected exceptionally well-preserved belemnites, compared to published $\delta^{18}O$ temperature reconstructions (Nunn et al., 2009, using the Anderson and Arthur, 1983 equation, assuming “normal” marine salinity of 34 PSU and $\delta^{18}O_{sw}$= -1 ‰), plotted against existing bio- and lithostratigraphic scheme for the Trotternish section (Hesselbo and Coe, 2000). Open circles on the Nunn et al. (2009) data indicate samples analysed for clumped isotopes in this study. Reconstructed $\delta^{18}O_{sw}$ data are shown on the left. Reconstructed $\delta^{18}O_{sw}$ calculated using the equations of Kim and O’Neil (1997) and Kele et al. (2015) are shown. L. Call = lower Callovian; MC = middle Callovian; UC = upper Callovian; L. Kimm. = lower Kimmeridgian Mbr = Member

Figure 6: Comparison of the reconstructed clumped isotope temperatures and $\delta^{18}O_{sw}$ from this study to those made using quantitative sporomorph data for the southern North Sea (Abbink et al., 2001), and clumped isotope temperatures for belemnites from the Russian Platform (Wierzbowski et al., 2018 Δ_{47} data; recalculated using the [*Brand*] isotopic parameters (Daëron et al., 2016) with the Wacker et al. (2014) calibration (pale blue and red); and converted to ETH values through ETH standards with "york regression" and converted to temperature using the Bernasconi et al., 2018 calibration, deep red blue and red). Seawater $\delta^{18}O$ was reconstructed using the equations of Kele et al. (2015; red and blue), and Kim and O'Neil (1997; pale blue and pink). εNd (t) data compilation for Euro-Boreal realm and Russian Platform from Dera et al. (2015).

Appendices

Appendix A: spreadsheet with the clumped isotope data and calculated $\delta^{18}O_{sw}$ presented in this study.

Appendix B: Supplementary μ-xrf and SEM data for selected belemnites.

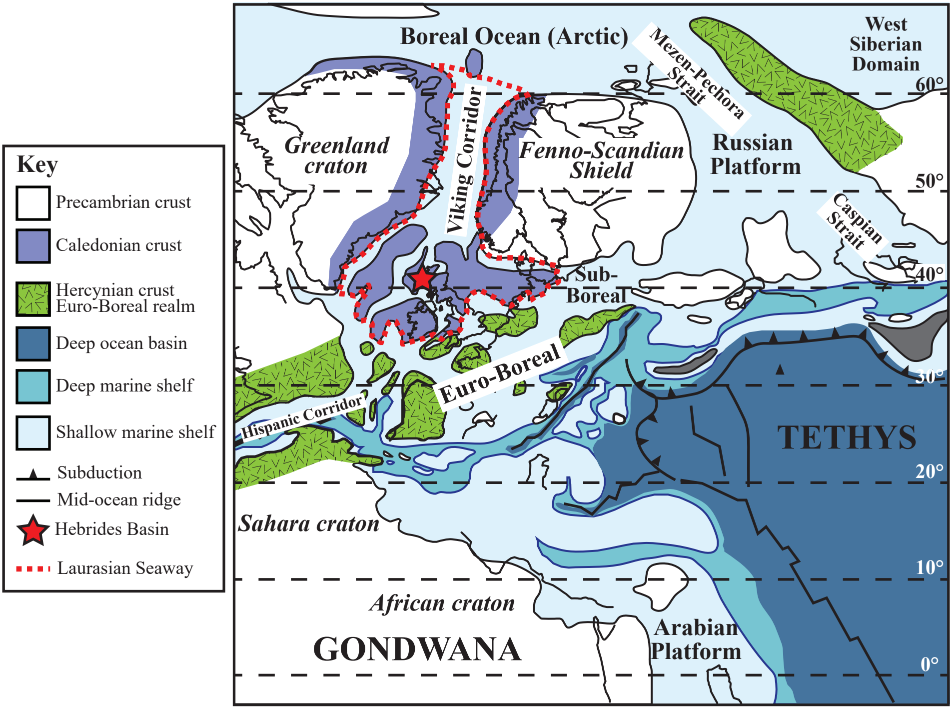

Key
Precambrian crust
Caledonian crust
Hercynian crust
Euro-Boreal realm
Deep ocean basin
Deep marine shelf
Shallow marine shelf
Subduction
Mid-ocean ridge
Hebrides Basin
Laurasian Seaway
Boreal Ocean (Arctic)
Mezen-Pechora Strait
West Siberian Domain
60°
Greenland craton
Viking Corridor
Fenno-Scandian Shield
Russian Platform
50°
Caspian Strait
Sub-Boreal
40°
Euro-Boreal
30°
Hispanic Corridor
TETHYS
20°
Sahara craton
10°
African craton
Arabian Platform
GONDWANA
0°

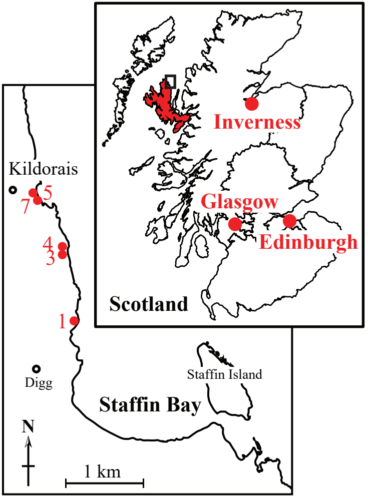

Inverness
Glasgow
Edinburgh
Scotland
Kildorais
5
7
4
3
1
Digg
Staffin Island
Staffin Bay
N
1 km

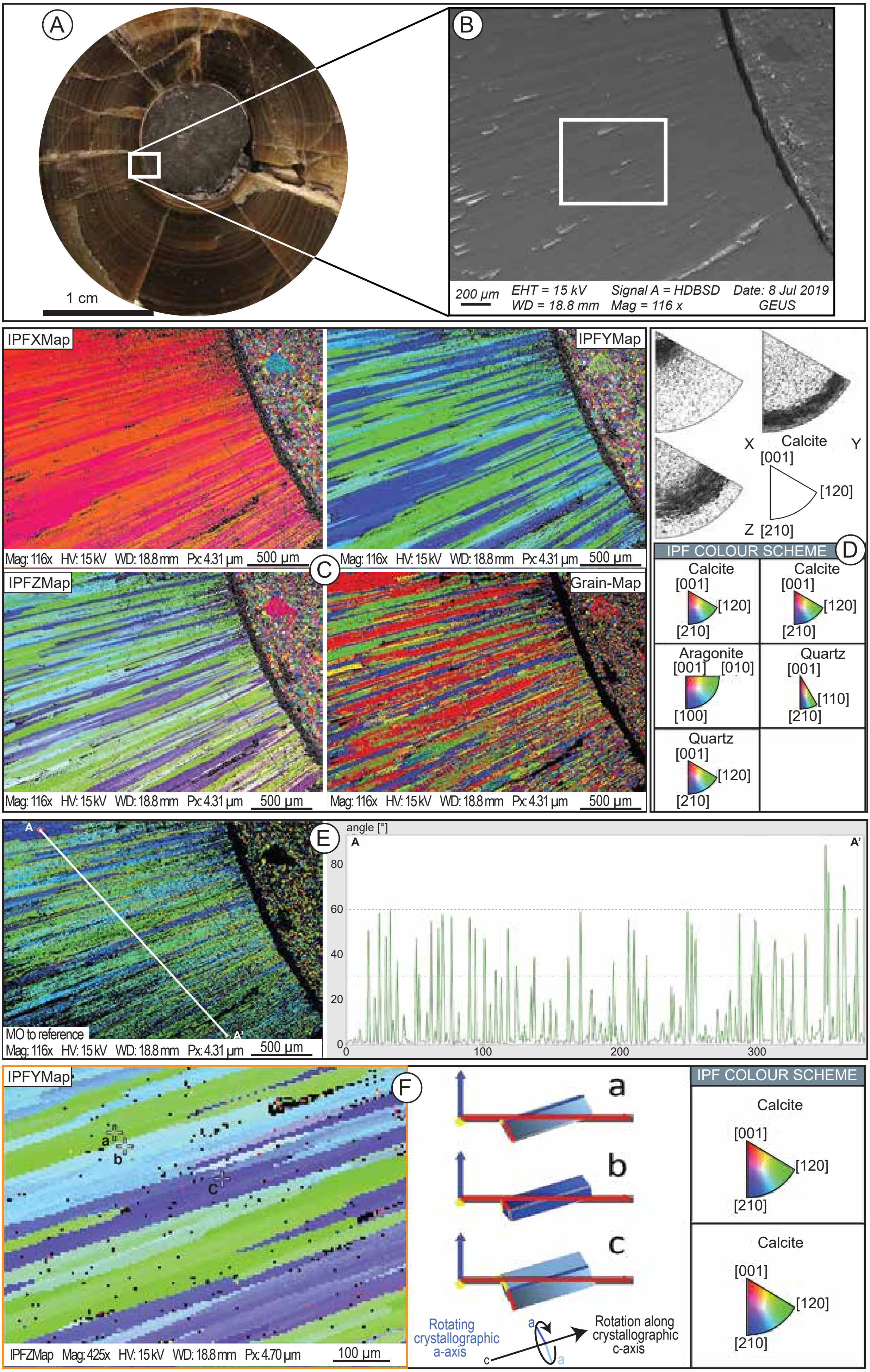

A
B
1 cm
200 µm
EHT = 15 kV
WD = 18.8 mm
Signal A = HDBSD
Mag = 116 x
Date: 8 Jul 2019
GEUS
IPFXMap
IPFYMap
IPFZMap
Grain-Map
Mag: 116x HV: 15 kV WD: 18.8 mm Px: 4.31 µm 500 µm
C
X
Calcite
Y
[001]
[120]
Z [210]
IPF COLOUR SCHEME
D
Calcite
Aragonite
[010]
[100]
Quartz
[110]
E
MO to reference
A
A'
angle [°]
F
a
b
c
IPFZMap Mag: 425x HV: 15 kV WD: 18.8 mm Px: 4.70 µm 100 µm
Rotating crystallographic a-axis
Rotation along crystallographic c-axis

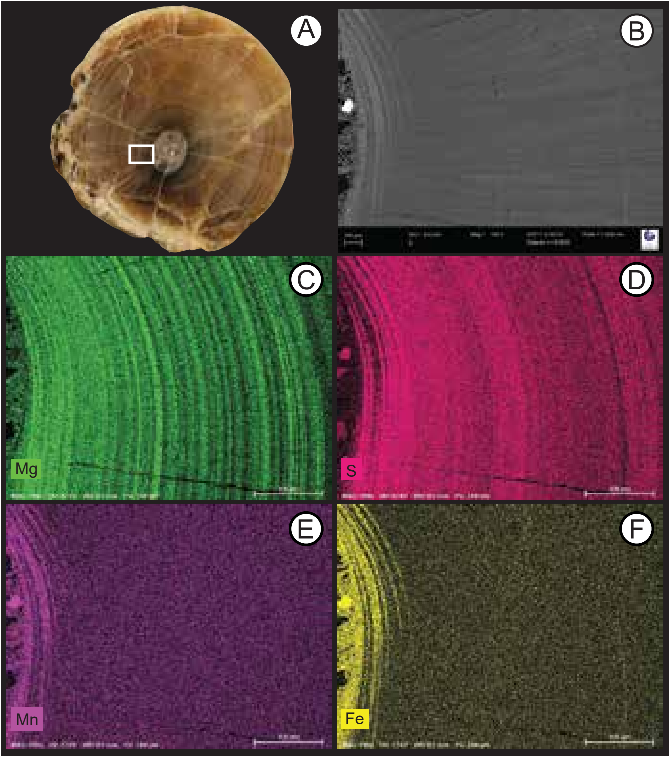
A
B
C
D
E
F
Mg
S
Mn
Fe

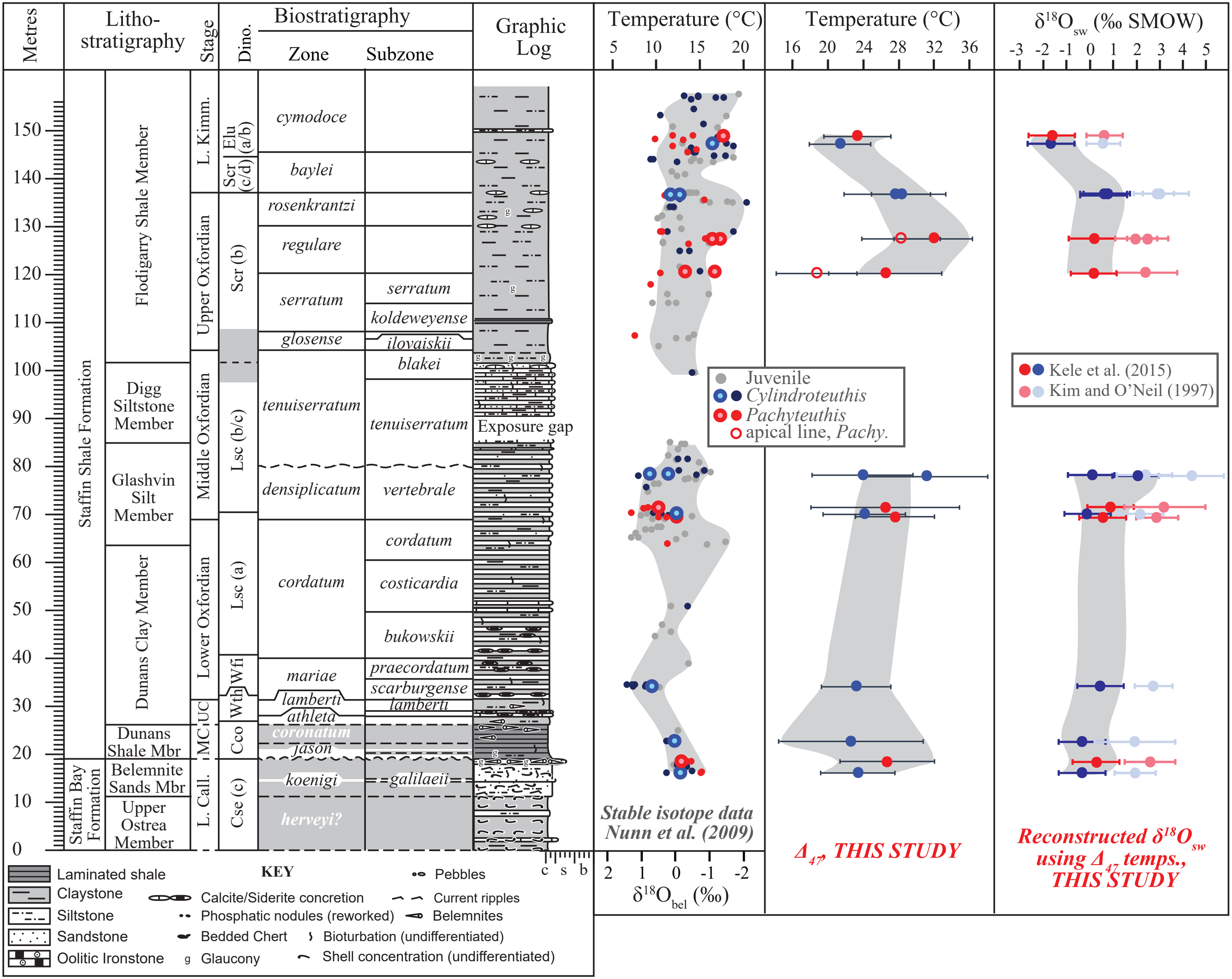

Metres
Litho-stratigraphy
Stage
Dino.
Biostratigraphy
Zone
Subzone
Graphic Log
Temperature (°C)
Temperature (°C)
$\delta^{18}O_{sw}$ (‰ SMOW)
Staffin Shale Formation
Flodigarry Shale Member
Digg Siltstone Member
Glashvin Silt Member
Dunans Clay Member
Dunans Shale Mbr
Staffin Bay Formation
Belemnite Sands Mbr
Upper Ostrea Member
L. Kimm.
Upper Oxfordian
Middle Oxfordian
Lower Oxfordian
L. Call.
cymodoce
baylei
rosenkrantzi
regulare
serratum
glosense
tenuiserratum
densiplicatum
cordatum
mariae
lamberti
athleta
coronatum
jason
koenigi
herveyi?
serratum
koldeweyense
ilovaiskii
blakei
tenuiserratum
vertebrale
cordatum
costicardia
bukowskii
praecordatum
scarburgense
lamberti
galilaeii
Exposure gap
Juvenile
Cylindroteuthis
Pachyteuthis
apical line, Pachy.
Kele et al. (2015)
Kim and O'Neil (1997)
Stable isotope data Nunn et al. (2009)
Δ_{47}, THIS STUDY
Reconstructed $\delta^{18}O_{sw}$ using Δ_{47} temps., THIS STUDY
$\delta^{18}O_{bel}$ (‰)
KEY
Laminated shale
Claystone
Siltstone
Sandstone
Oolitic Ironstone
Calcite/Siderite concretion
Phosphatic nodules (reworked)
Bedded Chert
Glaucony
Pebbles
Current ripples
Belemnites
Bioturbation (undifferentiated)
Shell concentration (undifferentiated)

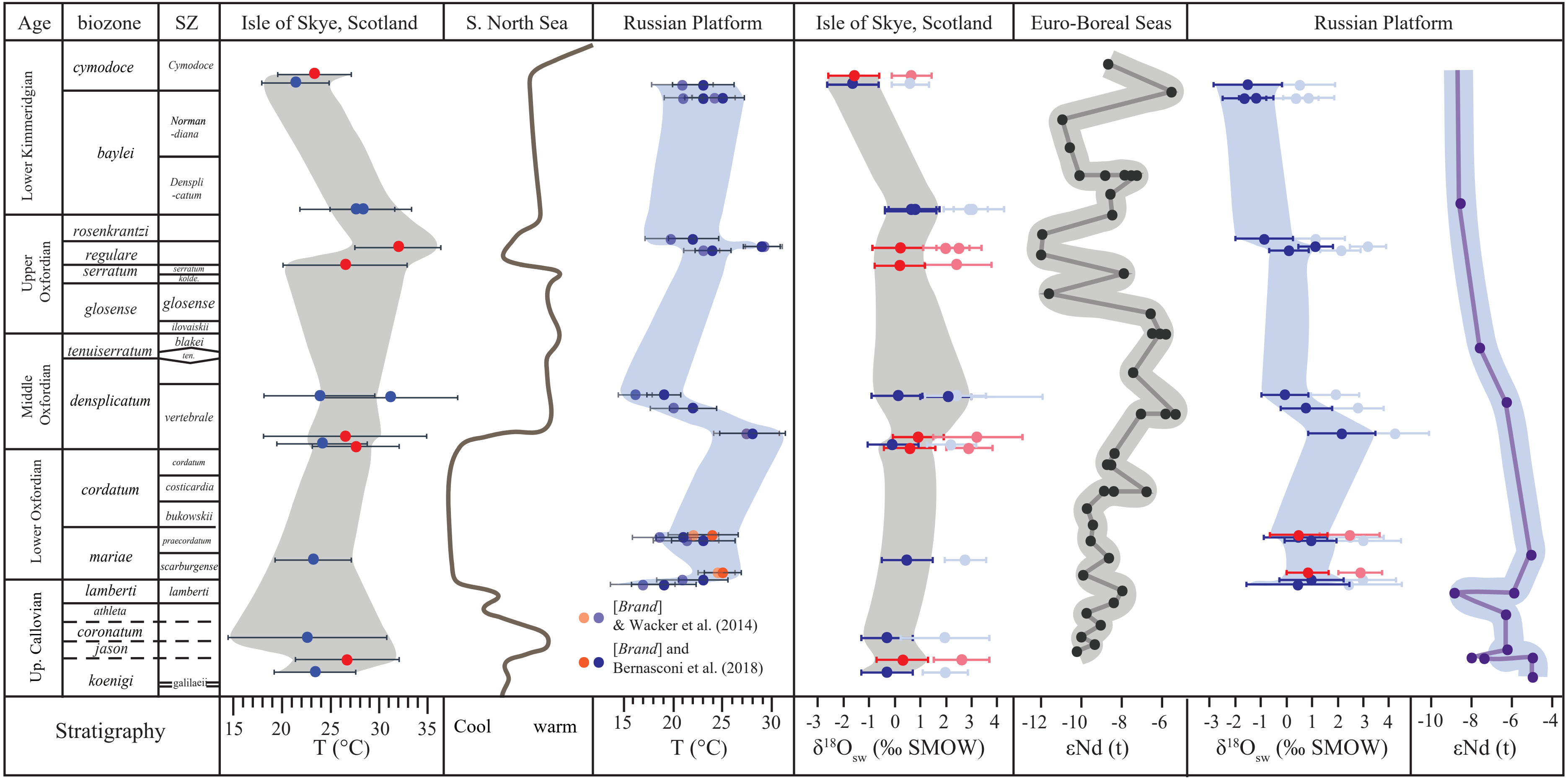

Age
biozone
SZ
Isle of Skye, Scotland
S. North Sea
Russian Platform
Isle of Skye, Scotland
Euro-Boreal Seas
Russian Platform
Lower Kimmeridgian
Upper Oxfordian
Middle Oxfordian
Lower Oxfordian
Up. Callovian
cymodoce
baylei
rosenkrantzi
regulare
serratum
glosense
tenuiserratum
densplicatum
cordatum
mariae
lamberti
athleta
coronatum
jason
koenigi
Cymodoce
Norman -diana
Denspli -catum
serratum
kolde.
glosense
ilovaiskii
blakei
ten.
vertebrale
cordatum
costicardia
bukowskii
praecordatum
scarburgense
lamberti
galilaeii
[Brand] & Wacker et al. (2014)
[Brand] and Bernasconi et al. (2018)
Stratigraphy
15 20 25 30 35
T (°C)
Cool warm
15 20 25 30
T (°C)
-3 -2 -1 0 1 2 3 4
δ18Osw (‰ SMOW)
-12 -10 -8 -6
εNd (t)
-3 -2 -1 0 1 2 3 4
δ18Osw (‰ SMOW)
-10 -8 -6 -4
εNd (t)